

Dynamic pressure variations in the lower crust caused by localized fluid-induced weakening

Evangelos Moulas^{1✉}, Boris Kaus¹ & Bjørn Jamtveit²

Metamorphism of dry, lower crust within orogens is often localized in shear zones composed of mechanically weaker rocks¹⁻⁴. Several field-based studies suggest shear zone development is preceded by brittle faults which provide the fluid pathways required for metamorphism and weakening⁴⁻¹². However, a unifying model which couples long-term geological deformation to fluid migration and metamorphic reactions does not exist. Here, we present a visco-elasto-plastic model where the most pertinent features observed in transformed lower crust emerge from basic mechanical principles during the deformation of a coherent rock volume with associated fluid introduction. These include a strikingly dynamic and heterogeneous pressure distribution in the reacting and deforming rock volumes. Lower crustal pressure variations may reach 1 GPa at the same depth. This will have first order effects on the pattern of fluid migration in the lower crust, and may explain the apparent discrepancies between the relevant tectonic settings and petrologically-inferred burial depths.

¹Institute of Geosciences, & Mainz Institute of Multiscale Modeling (M3ODEL), Johannes Gutenberg University Mainz, Mainz, Germany. ²The Njord Centre, Department of Geosciences, University of Oslo, Oslo, Norway. ✉email: evmoulas@uni-mainz.de

The lower crust was for a long time assumed to represent the weak layer of the continental lithosphere, sandwiched between a strong upper crust and mantle (the 'jelly sandwich model'¹³). Yet, during continent collision, earthquakes, although more frequent in the shallow crust, occur at all crustal levels (Fig. 1A)^{14,15}. Recently, Dunkel et al.¹⁶ reported textures indicative of seismic faulting in dry lower crustal rocks from the Lofoten Archipelago in the Northern Norwegian Caledonides, indicating very high (≥ 1 GPa) stress levels and therefore suggesting that the lower crust was strong, not weak¹⁷. Similar suggestions have been made also for other field areas where dry, lower-crustal lithologies occur^{18,19}. For the Bergen Arcs of Western Norway, such high stress levels were recently demonstrated directly by the presence of highly overpressured frictional melts along lower crustal faults²⁰.

When fluids are introduced into the lower crust along seismic faults, metamorphic reactions taking place in the damaged wall-rocks cause weakening and development of shear zones localized around the initial faults^{10,12}. In the Bergen Arcs of Western Norway (Fig. 1B) and the Lofoten Archipelago in Northern Norway, some of these shear-zones develop eclogite-facies mineral assemblages and appear to have formed at higher pressure than the pressures prevailing during faulting and shear zone initiation²¹. These high-pressure assemblages were initially assumed to have formed at an early stage near the bottom of an exceptionally thick crust. However, recent tectonic reconstructions, petrologic studies and new geochronological data from the Bergen Arcs indicate that the eclogite-facies shear zones formed synchronously with the development of amphibolite-facies shear zones in neighbouring outcrops^{22,23}. Based on these observations, a unifying mechanical model for lower crustal evolution during orogeny should explain both an early stage characterized by highly localized brittle deformation, often accompanied by fluid infiltration, and a later stage dominated by ductile deformation in hydrated shear zones with highly variable pressures at similar crustal levels. In particular, mechanical models that have been used to quantify pressure differences in viscously deforming rocks consider only idealized scenarios where the viscosity contrasts and the geometry are pre-defined^{8,21,24}. The orientation of planar structures, such as shear zones in this case, plays a dominant role on the sign of the pressure variations^{24,25}. Isolated shear zones having an acute angle to the far-field maximum compressive stress tend to develop negative pressure differences from the

surrounding matrix²⁴. In contrast, isolated shear zones at obtuse angles to the far-field maximum compressive stress develop positive overpressure values^{24,26}. Clearly, a rotation of the shear-zone network during finite-strain deformation is expected to induce changes in the sign of the pressure differences⁸. However, the pressure variations caused by viscosity heterogeneities scale proportionally to the effective viscosity contrast^{24,25,27}, which does not generally remain constant. Thus, models that predict the spontaneous formation, the finite-strain evolution, and the effective viscosity distribution in a shear zone network are needed in order to capture the temporal character of stress and pressure distribution.

The model presented below is based on previous works^{26,28}, which have demonstrated that the localization of brittle faults in pressure-sensitive materials leads to negative pressure deviations (underpressure) within the fault zones when compared to the surrounding matrix. These pressure differences can be preserved even after the localization of the fault, for as long as the damaged fault zone material remains mechanically weaker than the surrounding rock^{24,27,29}. The lower pressure experienced by brittle materials allows further localization of deformation and promotes fluid influx from the surroundings, if available. Fluid introduction to lower crustal rocks will invariably lead to metamorphic reactions and rheological weakening both due to a reduction in grain size and the formation of weaker hydrous minerals, such as micas^{2,8,30–33}. Sustained far-field (tectonic-) loading will then lead to viscous deformation and the development of shear zones along the weakened and reacted rock volumes¹². The shear zones effectively develop into volumes where the effective viscosity is lower than in its unreacted surrounding, i.e. weak zones (Fig. 1B).

Once a shear zone or a shear zone network has formed, the amount of finite strain can be very large and this can significantly reorient the original structure³⁴. Weak zones are expected to experience significant mean-stress variations. In this work, negative mean stress is taken as synonymous with pressure, thus, pressure variations are expected depending on orientation of the weak zones in the shear zone network^{8,28,35}. The maximum pressure values are expected when the elongated weak zones are oriented perpendicular to the direction of the maximum normal stress^{24,25}. More recent visco-elasto-plastic thermo-mechanical models have confirmed that the re-orientation of lithospheric-scale shear zones during finite deformation leads to a dynamic pressure evolution, independently of burial depth³⁶. Such

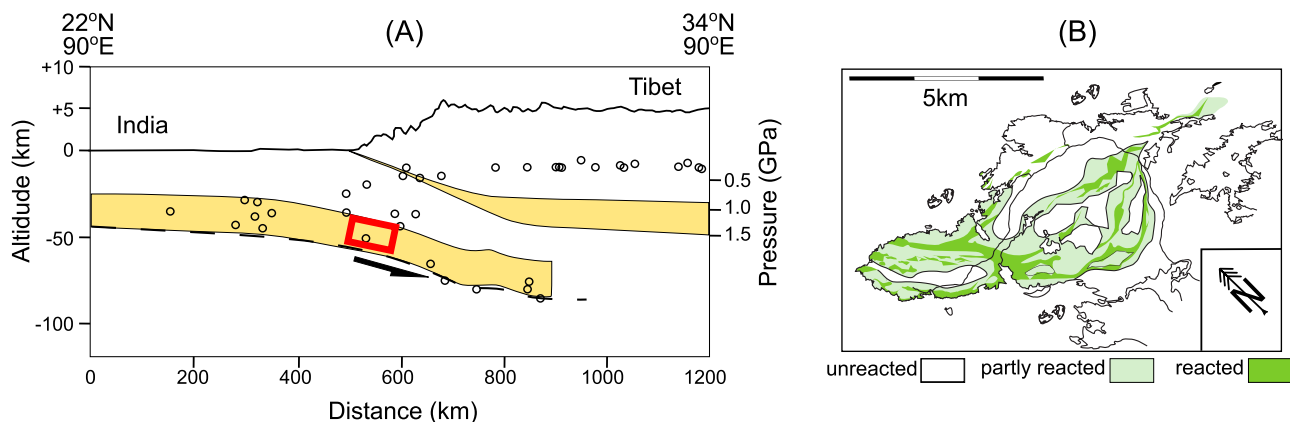


Fig. 1 Geophysical and field constraints on orogenic lower crust. Characteristics of lower crust during continent collision. **A** Distribution of earthquakes during the India-Asia collision exemplified by a cross-section along 90°E. Lower crust denoted by yellow color (modified from Jackson et al.¹⁵). Lithostatic pressures are given along the right vertical axis. The red rectangle indicates the Indian lower crust that experiences a lithostatic pressure of ca. 1.5 GPa. **B** Spatial distribution of reacted and unreacted rock volumes on the island of Holsnøy, Norway. The reacted zones correspond to highly deformed regions where the mineral assemblages suggest metamorphic pressures in the range 1–2 GPa (image modified from Austrheim, 2013¹, with permission from Elsevier).

pressure variations exert first-order control on the stable mineral assemblages³⁷. Indeed, it has been suggested that the local occurrence of ‘over-pressured’ rocks (eclogite) in shear zones in the Bergen arcs is the result of pressure perturbations associated with the formation of weak reacted volumes in strong, highly stressed, host rocks²¹. Despite the physical feasibility of such models, a self-consistent model that would predict and resolve the development of a shear zone network, as well as the subsequent dynamic development of both overpressured and underpressured regions, is still unavailable.

Results and Discussion

To analyze the mechanical conditions prevailing during tectonic compression of a lower crustal volume when subject to localized fluid-induced weakening, we have performed 2D high-resolution visco-elasto-plastic thermomechanical simulations of a 4×1 km region in the lower crust under shear (see *Methods* section for technical details). As a case study we have considered lower-crustal granulites from the Bergen Arcs in Western Norway (e.g. Figure 1B). These rocks recrystallized to form dry, lower-crustal granulites at ca 930 Ma³⁸ and experienced subsequent amphibolite to eclogite-facies (ca 1–2 GPa at 600–700 °C) conditions during the Caledonian orogeny at ca 425–430 Ma^{21,38}. Since plagioclase is by far the dominant mineral in the dry granulites, the initial creep rheology is represented by dry plagioclase¹⁷. A single weak inclusion (wet plagioclase rheology¹⁷) is added at the bottom of the model domain to trigger localized deformation. This inclusion is assumed to be connected to an external fluid (water-) reservoir located immediately below the model, to simulate the field situation of the Lindås Nappe in the Bergen Arcs where dry granulites are thrust upon Paleozoic sedimentary rocks undergoing prograde, fluid-producing, metamorphism²².

With ongoing deformation, stresses build up until the yield stress is reached. Field observations demonstrate that this is followed by dynamic rupturing and highly localized seismic slip^{19,39}. Associated wall rock damage allows fluid infiltration, metamorphic hydration reaction, and mechanical weakening of a 0.1–1 m wide zone of wall rocks⁸. The details of these processes cannot be described within the temporal and spatial resolution of our model. We therefore parameterize this by changing the rheology from dry to wet plagioclase once an accumulated plastic strain of 10% is reached in our model (see *Methods* for more details). Figure 2 shows the output of our simulations for a constant sinistral shear strain rate of $5 \times 10^{-15} \text{ s}^{-1}$ after 7 million years. We observe striking and dynamic variations in stress, deformation rate and pressure (= mean stress) in the deforming lower crust (see also Supplementary Notes 3). Maximum pressure variations within the model domain approach 1 GPa, with local and continuous pressure gradients that may exceed the lithostatic pressure gradient by a factor of ~30. Even within low-viscosity shear zones, significant along-shear zone variations in dynamic pressure occur, with intermittent high-pressure values frequently occurring at the intersection of shear zones. Pressure magnitudes depend on orientation with respect to the overall kinematic deformation and the local state of stress (which evolves depending on the presence of other shear zones). The resulting shear zone pattern is complex and consists of both small-scale and large-scale deformation zones, with the widest being internally heterogeneously deformed.

In order to investigate the sensitivity of our model to our model parameters, we have performed systematic simulations in which we varied the background strain rate, the temperature, the weakening parameters and the numerical resolution (Supplementary Notes 4). Results are generally consistent for all reasonable choices of input parameters. Second order variations occur due to strain weakening and the critical hydration strain,

i.e. the strain value where the damaged rocks become effectively weaker and they are approximated by a ‘wet’ flow law. The timing is to a large extent controlled by the applied background strain rate. A primary requirement, however, is that the background viscosity and deformation rate are such that the brittle yield stress is reached. Simulations under conditions where this is not the case, for example because the temperature is higher (e.g., 700 °C instead of 650 °C, for a strain rate of $5 \times 10^{-15} \text{ s}^{-1}$) are shown in the supplementary notes (Supplementary Notes 4, Fig. S3a). Field observations from a variety of localities, including the Norwegian Caledonides, the Alps, the Musgrave ranges and the Himalayan-Tibetan orogen, do however indicate that brittle deformation is common in lower crustal volumes during plate convergence^{12,40}.

Our results are consistent with previous work emphasizing that lower crustal shear zones originate by brittle failure^{12,40}. Importantly, this leads to a drop in pressure within the highly localized shear zone compared to the surrounding matrix^{26,28,41,42}. Hydration weakening further enhances the viscosity variations, resulting in larger stress and pressure variations within the system. It is also interesting to note that the local sense of shear within many of these shear zones appears inconsistent with the overall applied background kinematic deformation rate. This is in agreement with previous studies of the formation of brittle and ductile shear zones⁴³ and is caused by local changes in the principal stress direction.

To analyze the petrological consequences of the inferred pressure variations, we performed phase equilibrium calculations to identify the stable mineral assemblages for a typical granulite from Holsnøy as a function of the pressure and temperature (P-T) conditions (Fig. 3A). For the calculation we used the measured loss on ignition (LOI) as an upper bound of the H₂O content of these rocks. Since it is expected that the presence of water will facilitate mineral reactions, our equilibrium phase equilibria calculations are relevant only for the reacted and the partly reacted zones characterized by the presence of hydrous minerals and/or recrystallized material^{1,8,44}.

It is expected that a limited amount of H₂O in the rock may be insufficient to saturate the system with respect to a free H₂O fluid phase. Figure 3B shows the amount of water required for saturation at 650 °C, a temperature relevant for the Holsnøy situation based on previous work^{21,45}, as a function of pressure (see details on *Methods*). For pressures in the range 1–2 GPa, Fig. 3B shows that a pressure increase will tend to stabilize hydrous assemblages and absorb any free H₂O that may have been available at lower pressures. Hence, high pressure reacting regions may, counterintuitively, act as fluid sinks rather than sources. This result is not limited to a particular composition, and it is relevant for similar systems that experience dehydration reactions exhibiting positive slopes in the P-T space.

Spatial and temporal variation in pressure may have first order effects both on the rheological and petrological evolution of the lower crust. The pressure drop associated with initial brittle failure would naturally draw in water from any external water reservoir. Hence, this effect would naturally couple retrograde fluid-consuming metamorphism of dry rocks to spatially associated volumes undergoing prograde, fluid-producing, metamorphism. Relevant geological scenarios from collisional orogens, exemplified by the Lindås Nappe in the Bergen Arcs, include thrusting of lower crustal units over a footwall containing lower grade metasedimentary rocks²³. Continuous pressure gradients that may exceed the lithostatic gradient by over an order of magnitude would furthermore act as an effective local distribution system for fluids, with the additional complexity that reacting volumes that are about to run out of fluid would act as fluid sinks even if the rock pressure remains high⁴⁶.

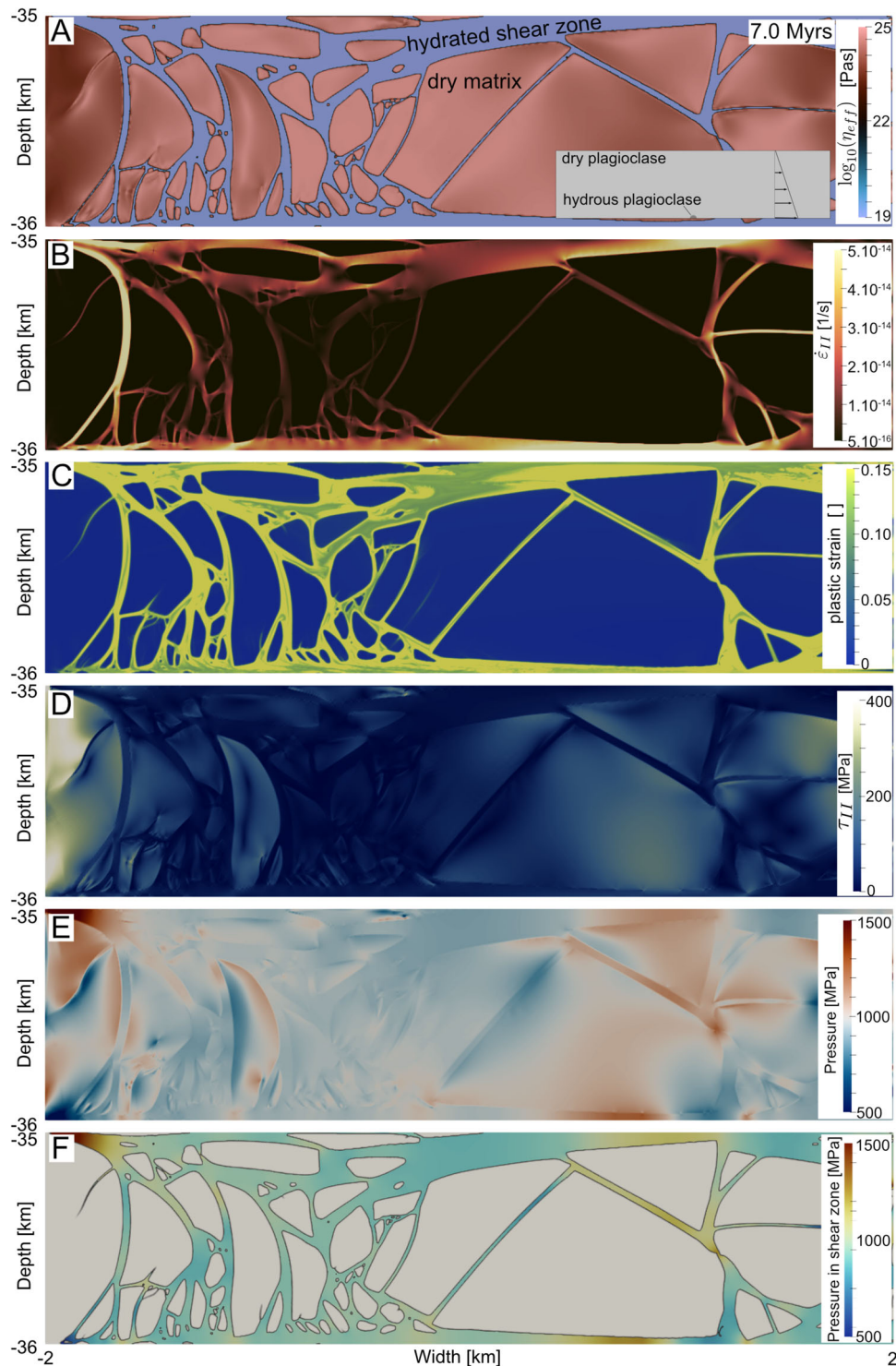


Fig. 2 Numerical simulation of the formation hydrated shear zones in the lower crust. The simulation, using a grid resolution of 4m^2 , started with an initially homogeneous, dry, lower crust (at $650\text{ }^\circ\text{C}$) with a single embedded wet-plagioclase-dominated inclusion (inset in A). When imposing a constant, sinistral shear strain rate of $5 \times 10^{-15}\text{ s}^{-1}$, brittle shear zones develop, followed by hydrated, weak, shear zones. Shown are snapshots that illustrate **A** effective viscosity, **B** second invariant of strain rate tensor, **C** second invariant of plastic strain, **D** second invariant of the deviatoric stress tensor, **E** dynamic pressure, and **F** detail of dynamic pressure within the shear zones. Complex shear zone patterns emerge that have significant variations in stresses and dynamic pressures and may explain the coexistence of high and lower pressure assemblages in the same rocks. See Supplementary Movies S1-4 (Supplementary Notes 3) for animation and (Fig. S1, Supplementary Notes 2; Fig. S7, Supplementary Notes 4) for the temporal evolution for a range of imposed strain rates.

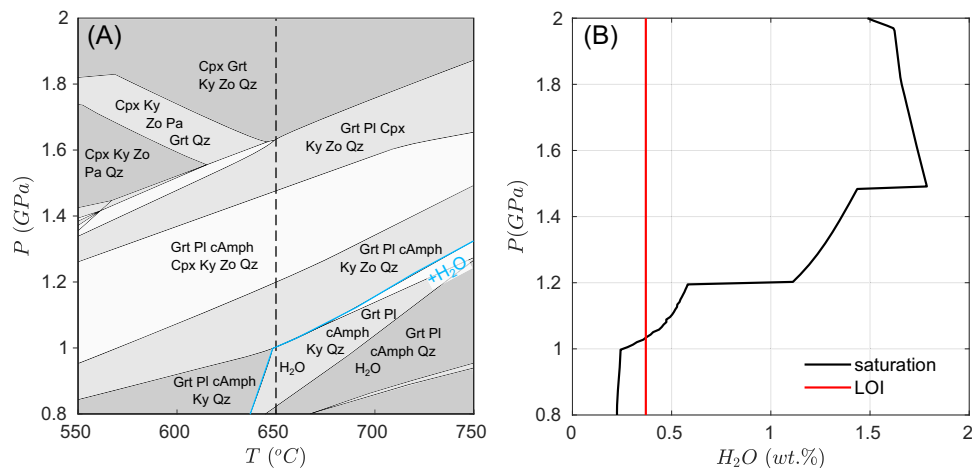


Fig. 3 Phase diagram section for a representative granulite from Holsnøy. The phase diagram section has been calculated via Gibbs-free energy minimization by assuming a fixed amount of H₂O (see Methods for more details). **A** Equilibrium mineral assemblages for the granulite from Holsnøy (mineral abbreviations: Cpx: clinopyroxene, Grt: garnet, Ky: Kyanite, Zo: zoisite, cAmph: clinoamphibole, Pl: plagioclase feldspar, Qz: quartz, Pa: paragonite mica, H₂O: pure H₂O fluid). **B** The black solid line shows the amount of H₂O needed for water-saturation, i.e. fluid-present conditions (the assumed temperature conditions (650 °C) are indicated by dashed line in (A)). The red line indicates the amount of H₂O (LOI) that was also used for the calculation of the pressure-temperature section (shown in A). The intersection and relative positions of the black and red lines in (B) shows that the H₂O content is sufficient to saturate the system only in a pressure range below ~1.0 GPa. For the pressure range between 1–2 GPa, the rock is H₂O-undersaturated and no free H₂O phase is stable.

The presence of pressure variations imposed by mechanical processes, as described above, is highly relevant for the interpretation of the pressures recorded by metamorphic mineral assemblages in terms of underlying tectonic scenario^{25,47–49}. In our modelling scenario, high-pressure (≈ 2 GPa) assemblages would locally form without the necessity of excessively deep burial of the relatively low density granulites. At the same time, abundant underpressurized (≈ 1 GPa) regions would form at more or less similar depths. Traditionally these rocks would be interpreted to have formed at some later stage following 20–40 km of crustal exhumation. Hence, our model has radical consequences for the interpretation of metamorphic mineral assemblages in terms of the underlying geodynamic processes.

High (≈ 1 GPa) differential stress levels in the dry lower crust have important consequences for its rheological and physico-chemical evolution. Under high stress, the deformation of the lower crust is dominated by plastic shear bands that will provide the available pathways for any external fluid phase. Following fluid-introduction at high temperatures, the shear bands will evolve into a shear-zone network where rocks behave in a viscoplastic manner. The model presented above naturally produces shear zone networks (Fig. 2, and movies in Supplementary Notes 3) at a similar scale and with similar geometry to what is observed at Holsnøy in the Bergen Arcs (Fig. 1B). As the lower crustal rheology changes from that of dry and strong granulites to that of weaker eclogites and amphibolites, a characteristic pattern develops where rounded blocks of strong granulites are displaced along growing hydrated shear zones that reflect a range of metamorphic pressure conditions. This large range of metamorphic pressure conditions may thus not always reflect metastability and can be explained by the particular mechanical configuration.

Methods

Thermo-mechanical simulations. We performed 2D simulations using LaMEM, which solves the conservation equations for mass, energy and momentum of slowly moving rocks using a staggered grid finite difference method combined with a marker-and-cell approach^{50,51}. We employ a temperature-dependent visco-elasto-plastic rheology, where dislocation creep is combined with non-associated

Drucker-Prager plasticity. We have implemented a regularized plasticity⁵². More details on all employed material parameters are given in the supplementary notes 1.

Properties are tracked on markers that are mapped to the computational grid in a conservative manner⁵³. A constant value of 1000 MPa is added to the pressure value to take into account that our model domain is at around 35 km depth within the crust. A uniform constant density of 3000 kg/m³ is assumed in our model and therefore the effects of gravity are limited to the generation of a uniform lithostatic pressure gradient. For simplicity, we assume a constant temperature within the model domain with flux-free lateral thermal boundaries and isothermal upper and lower boundaries. In order to simulate the shear induced by a subducting slab moving underneath the crust (see Fig. 1), we apply kinematic velocity boundary conditions in which we move the lower boundary to the right and keep the upper boundary fixed, such that a constant background shear strain rate of $5 \times 10^{-15} \text{ s}^{-1}$ is achieved in our reference simulation. The side boundaries are kinematically prescribed, which induces stress heterogeneities at the lateral boundaries that initiate shear zones similar to what would happen if small heterogeneities in material strength were taken into account. Brittle localization results from non-associated plasticity, while the effect of damaging rocks is taken into account through frictional strain softening that linearly lowers both the friction angle and cohesion between an accumulated plastic strain of 0.01 and 0.1 until it is reduced by 90% of its initial value, while normalized for a fault thickness of 10 m (see Supplementary Notes 4 for variations of this; Fig. S5a,b).

Water migration through shear zones is a process that is fast compared to the typical time step of our model. Its main mechanical effect is to change the rheology of the rocks once the shear zones become hydrated. We parameterize this effect by changing the rheology from dry to wet plagioclase once an accumulated plastic strain (critical hydration strain) of 0.1 is reached. This value is based on the cumulative value of the second invariant of the plastic strain rate. The reason for this choice lies in the fact that, in the presence of fluids, metamorphic reactions can occur at laboratory timescales for temperatures of 600 °C and higher⁵⁴. As a consequence, the weakening is expected to occur almost instantaneously when compared to the geological deformation rates that are modeled in this work. A critical value of plastic strain (e.g. 0.1) is chosen since pressure differences at nucleating plastic shear bands are proportional to strain⁴². Furthermore, with progressive strain, it is expected that isolated microcracks (below the limit of our resolution) will interconnect⁵⁵. Both the underpressure development and the micro-fracture interconnection will enhance the fluid supply needed for the relatively instantaneous hydration reactions. A systematic investigation of the value of the critical plastic strain showed that different values produce very similar results (see Supplementary Notes 4 for variations in this parameter; Fig. S6a,b). To prevent material that flows in from the left boundary from being instantly weakened, we set the accumulated plastic strain of inflowing markers to zero. This feature has been chosen as a better approximation for deformation in subduction settings compared to periodic boundary conditions.

We apply the Flexible-GMRES Krylov method to solve the governing incompressible Stokes equations, preconditioned with a direct LU solver and a penalty term on the pressure block. We configure the models with 27 markers per control volume to set the material properties and temperature structure. LaMEM is

written on top of PETSc⁵⁶ and utilizes SNES nonlinear solver framework. The nonlinear SNES solver has a convergence criterion that is either a relative tolerance (rtol) of 10^{-4} or absolute tolerance (atol) of 10^{-7} and we employ the Eisenstat-Walker algorithm, combined with line search (l2). The inner linear KSP solver is terminated when a relative tolerance of 10^{-3} , an absolute tolerance of 10^{-10} , or 100 iterations are reached.

We have performed a total of over 50 simulations to better understand the dynamics of the system, and the sensitivity of the results to the model parameters (see Supplementary Notes 4). Whereas details of the simulations, such as the number of shear zones are a function of the material parameters, the overall conclusions with respect to the dynamic stress and pressure variations are robust.

LaMEM is open-source software and available at <https://bitbucket.org/bkaus/lamem>. Detailed instructions and scripts to reproduce the results presented are uploaded to zenodo (<https://zenodo.org/record/6538290>)⁵⁷.

Equilibrium Phase diagram sections. We performed phase equilibrium calculations by minimizing the Gibbs-free energy in the $\text{Na}_2\text{O-CaO-FeO-MgO-Al}_2\text{O}_3\text{-SiO}_2\text{-H}_2\text{O}$ model system. We used the Perple_X collection of programs^{58–60} and the hp02ver.dat thermodynamic database⁶¹ to construct isochemical pressure-temperature (P-T), phase-diagram sections. The bulk composition that was used is (in wt.%): Na_2O : 4.53, CaO : 9.88, FeO : 2.74, MgO : 2.33, Al_2O_3 : 25.96, SiO_2 : 53.34 and H_2O : 0.37 and the solid solutions that were considered are: “cAmph(DP)” for clinopyroxene, “Omph(GHP)” for clinopyroxene, “feldspar” for plagioclase feldspar, “Opx(HP)” for orthopyroxene, “Gt(GCT)” for garnet and “Chl(W)” for chlorite (details for the solution models can be found in the solution_model.dat file in the following link http://www.perplex.ethz.ch/perplex/ibm_and_mac_archives/Perple_X_6.9.0_data_files.zip).

For the calculation of the amount of water needed for saturation, a P-T section was calculated for a sufficiently large amount of H_2O (e.g. 20% wt.) by keeping the proportions of the other elements the same. The saturation amount was calculated as the amount of H_2O that is bounded in the mineral phases (as OH). The CORK H_2O equation of state was used in all the calculations^{61,62}.

Data availability

The authors confirm that the data supporting the findings of this study are available within the article and its supplementary information (see also Methods section). Detailed instructions and scripts to reproduce the results presented in Fig. 2 are uploaded to zenodo (<https://zenodo.org/record/6538290>).

Received: 21 March 2022; Accepted: 16 June 2022;

Published online: 08 July 2022

References

- Austrheim, H. Fluid and deformation induced metamorphic processes around Moho beneath continent collision zones: Examples from the exposed root zone of the Caledonian mountain belt, W-Norway. *Tectonophysics* **609**, 620–635 (2013).
- Jamtveit, B., Austrheim, H. & Putnis, A. Disequilibrium metamorphism of stressed lithosphere. *Earth-Science Reviews* **154**, 1–13 (2016).
- Labrousse, L., Hetényi, G., Raimbourg, H., Jolivet, L. & Andersen, T. B. Initiation of crustal-scale thrusts triggered by metamorphic reactions at depth: Insights from a comparison between the Himalayas and Scandinavian Caledonides. *Tectonics* **29**, (2010).
- Menegon, L., Pennacchioni, G., Malaspina, N., Harris, K. & Wood, E. Earthquakes as Precursors of Ductile Shear Zones in the Dry and Strong Lower Crust. *Geochemistry, Geophysics, Geosystems* **18**, 4356–4374 (2017).
- Newton, R. C. Fluids and shear zones in the deep crust. *Tectonophysics* **182**, 21–37 (1990).
- Austrheim, H. & Boundy, T. M. Pseudotachylytes Generated During Seismic Faulting and Eclogitization of the Deep Crust. *Science* **265**, 82 (1994).
- Putnis, A., Jamtveit, B. & Austrheim, H. Metamorphic Processes and Seismicity: the Bergen Arcs as a Natural Laboratory. *Journal of Petrology* **58**, 1871–1898 (2017).
- Kaatz, L. et al. Widening of Hydrated Shear Zones During Incipient Eclogitization of Metastable Dry and Rigid Lower Crust—Holsnøy, Western Norway. *Tectonics* **40**, e2020TC006572 (2021).
- Papa, S., Pennacchioni, G., Angel, R. J. & Faccenda, M. The fate of garnet during (deep-seated) coseismic frictional heating: The role of thermal shock. *Geology* **46**, 471–474 (2018).
- Incel, S., Renner, J. & Jamtveit, B. Evolution of Brittle Structures in Plagioclase-Rich Rocks at High-Pressure and High-Temperature Conditions—Linking Laboratory Results to Field Observations. *Geochemistry, Geophysics, Geosystems* **21**, e2020GC009028 (2020).
- Mancktelow, N. S. & Pennacchioni, G. The control of precursor brittle fracture and fluid–rock interaction on the development of single and paired ductile shear zones. *Journal of Structural Geology* **27**, 645–661 (2005).
- Jamtveit, B. et al. The Effects of Earthquakes and Fluids on the Metamorphism of the Lower Continental Crust. *Journal of Geophysical Research: Solid Earth* **124**, 7725–7755 (2019).
- Chen, W.-P. & Molnar, P. Focal depths of intracontinental and intraplate earthquakes and their implications for the thermal and mechanical properties of the lithosphere. *Journal of Geophysical Research: Solid Earth* **88**, 4183–4214 (1983).
- Jackson, J. A. Strength of the continental lithosphere: time to abandon the jelly sandwich. *GSA Today* **12**, 4–10 (2002).
- Jackson, J. A., Austrheim, H., McKenzie, D. & Priestley, K. Metastability, mechanical strength, and the support of mountain belts. *Geology* **32**, 625–628 (2004).
- Dunkel, K. G., Zhong, X., Arnestad, P. F., Valen, L. V. & Jamtveit, B. High transient stress in the lower crust: Evidence from dry pseudotachylytes in granulites, Lofoten Archipelago, northern Norway. *Geology* **49**, 135–139 (2020).
- Bürgmann, R. & Dresen, G. Rheology of the Lower Crust and Upper Mantle: Evidence from Rock Mechanics, Geodesy, and Field Observations. *Annu. Rev. Earth Planet. Sci.* **36**, 531–567 (2008).
- Hawemann, F., Mancktelow, N., Wex, S., Pennacchioni, G. & Camacho, A. Fracturing and crystal plastic behaviour of garnet under seismic stress in the dry lower continental crust (Musgrave Ranges, Central Australia). *Solid Earth* **10**, 1635–1649 (2019).
- Mancktelow, N. S., Camacho, A. & Pennacchioni, G. Time-Lapse Record of an Earthquake in the Dry Felsic Lower Continental Crust Preserved in a Pseudotachylyte-Bearing Fault. *Journal of Geophysical Research: Solid Earth* **127**, e2021JB022878 (2022).
- Zhong, X. et al. Lower crustal earthquake associated with highly pressurized frictional melts. *Nature Geoscience* **14**, 519–525 (2021).
- Jamtveit, B. et al. High Pressure Metamorphism Caused by Fluid Induced Weakening of Deep Continental Crust. *Scientific Reports* **8**, 17011 (2018).
- Jamtveit, B. et al. Rapid fluid-driven transformation of lower continental crust associated with thrust-induced shear heating. *Lithos* **396–397**, 106216 (2021).
- Putnis, A., Moore, J., Prent, A. M., Beinlich, A. & Austrheim, H. Preservation of granulite in a partially eclogitized terrane: Metastable phenomena or local pressure variations? *Lithos* **400–401**, 106413 (2021).
- Moulas, E., Burg, J.-P. & Podladchikov, Y. Stress field associated with elliptical inclusions in a deforming matrix: Mathematical model and implications for tectonic overpressure in the lithosphere. *Tectonophysics* **631**, 37–49 (2014).
- Mancktelow, N. S. Tectonic pressure: Theoretical concepts and modelled examples. *Lithos* **103**, 149–177 (2008).
- Mancktelow, N. S. How ductile are ductile shear zones? *Geology* **34**, 345–348 (2006).
- Schmid, D. W. & Podladchikov, Y. Y. U. Analytical solutions for deformable elliptical inclusions in general shear. *Geophysical Journal International* **155**, 269–288 (2003).
- Casey, M. Mechanics of shear zones in isotropic dilatant materials. *Journal of Structural Geology* **2**, 143–147 (1980).
- Rice, J. R. Fault Stress States, Pore Pressure Distributions, and the Weakness of the San Andreas Fault. in *Fault Mechanics and Transport Properties of Rocks* 475–503 (Academic Press, 1992).
- Jolivet, L. et al. Softening triggered by eclogitization, the first step toward exhumation during continental subduction. *Earth and Planetary Science Letters* **237**, 532–547 (2005).
- Schmalholz, S. M., Moulas, E., Plümper, O., Myasnikov, A. V. & Podladchikov, Y. Y. 2D Hydro-Mechanical-Chemical modelling of (de) hydration reactions in deforming heterogeneous rock: The periclase-brucite model reaction. *Geochemistry, Geophysics, Geosystems* **n/a**, e2020GC009351 (2020).
- Hirauchi, K., Fukushima, K., Kido, M., Muto, J. & Okamoto, A. Reaction-induced rheological weakening enables oceanic plate subduction. *Nature Communications* **7**, 12550 (2016).
- Bras, E., Bâisset, M., Yamato, P. & Labrousse, L. Transient weakening during the granulite to eclogite transformation within hydrous shear zones (Holsnøy, Norway). *Tectonophysics* 229026 <https://doi.org/10.1016/j.tecto.2021.229026> (2021).
- Escher, A., Escher, J. C. & Watterson, J. The Reorientation of the Kangamiut Dike Swarm, West Greenland. *Can. J. Earth Sci.* **12**, 158–173 (1975).
- Mancktelow, N. S. Finite-element modelling of shear zone development in viscoelastic materials and its implications for localisation of partial melting. *Journal of Structural Geology* **24**, 1045–1053 (2002).
- Schmalholz, S. M. & Podladchikov, Y. Y. Tectonic overpressure in weak crustal-scale shear zones and implications for the exhumation of high-pressure rocks. *Geophysical Research Letters* **40**, 1984–1988 (2013).

37. Moulas, E. et al. Relation between mean stress, thermodynamic, and lithostatic pressure. *Journal of Metamorphic Geology* **37**, 1–14 (2019).
38. Bingen, B., Davis, W. J. & Austrheim, H. Zircon U–Pb geochronology in the Bergen arc eclogites and their Proterozoic protoliths, and implications for the pre-Scandian evolution of the Caledonides in western Norway. *GSA Bulletin* **113**, 640–649 (2001).
39. Petley-Ragan, A. et al. Dynamic earthquake rupture in the lower crust. *Science Advances* **5**, eaaw0913 (2019).
40. Hawemann, F., Mancktelow, N. S., Pennacchioni, G., Wex, S. & Camacho, A. Weak and Slow, Strong and Fast: How Shear Zones Evolve in a Dry Continental Crust (Musgrave Ranges, Central Australia). *Journal of Geophysical Research: Solid Earth* **124**, 219–240 (2019).
41. Le Pourhiet, L. Strain localization due to structural softening during pressure sensitive rate independent yielding. *Bulletin de la Société Géologique de France* **184**, 357–371 (2013).
42. Duretz, T., Souche, A., de Borst, R. & Le Pourhiet, L. The Benefits of Using a Consistent Tangent Operator for Viscoelastoplastic Computations in Geodynamics. *Geochemistry, Geophysics, Geosystems* **19**, 4904–4924 (2018).
43. Meyer, S. E., Kaus, B. J. P. & Passchier, C. Development of branching brittle and ductile shear zones: A numerical study. *Geochemistry, Geophysics, Geosystems* **18**, 2054–2075 (2017).
44. Austrheim, H. Eclogitization of lower crustal granulites by fluid migration through shear zones. *Earth and Planetary Science Letters* **81**, 221–232 (1987).
45. Glodny, J., Kühn, A. & Austrheim, H. Geochronology of fluid-induced eclogite and amphibolite facies metamorphic reactions in a subduction–collision system, Bergen Arcs, Norway. *Contributions to Mineralogy and Petrology* **156**, 27–48 (2008).
46. Malvoisin, B. et al. Sustainable densification of the deep crust. *Geology* **48**, 673–677 (2020).
47. Petrini, K. & Podladchikov, Y. Lithospheric pressure–depth relationship in compressive regions of thickened crust. *Journal of Metamorphic Geology* **18**, 67–77 (2000).
48. Moulas, E., Podladchikov, Y. Y., Aranovich, L. Y. & Kostopoulos, D. K. The problem of depth in geology: When pressure does not translate into depth. *Petrology* **21**, 527–538 (2013).
49. Bauville, A. & Yamato, P. Pressure-to-Depth Conversion Models for Metamorphic Rocks: Derivation and Applications. *Geochemistry, Geophysics, Geosystems* **22**, e2020GC009280 (2021).
50. Kaus, B. J. P. et al. Forward and inverse modelling of lithospheric deformation on geological timescales. *NIC Series* **48**, 299–307 (2016).
51. Reuber, G. S., Kaus, B. J. P., Popov, A. A. & Baumann, T. S. Unraveling the Physics of the Yellowstone Magmatic System Using Geodynamic Simulations. *Frontiers in Earth Science* **6**, 117 (2018).
52. Duretz, T., de Borst, R., Yamato, P. & Le Pourhiet, L. Toward Robust and Predictive Geodynamic Modeling: The Way Forward in Frictional Plasticity. *Geophysical Research Letters* **47**, e2019GL086027 (2020).
53. Pusok, A. E., Kaus, B. J. P. & Popov, A. A. On the Quality of Velocity Interpolation Schemes for Marker-in-Cell Method and Staggered Grids. *Pure and Applied Geophysics* **174**, 1071–1089 (2017).
54. Incel, S. et al. Laboratory earthquakes triggered during eclogitization of lawsonite-bearing blueschist. *Earth and Planetary Science Letters* **459**, 320–331 (2017).
55. Segall, P. & Simpson, C. Nucleation of ductile shear zones on dilatant fractures. *Geology* **14**, 56–59 (1986).
56. Balay, S. et al. PETSc Users Manual. (2020).
57. Moulas, E., Kaus, B. J. P. & Jamtveit, B. Dynamic Pressure Variations in the Lower Crust Caused by Localized Fluid-Induced Weakening (LaMEM input files). *Zenodo* <https://doi.org/10.5281/zenodo.6538290> (2022).
58. Connolly, J. A. D. Computation of phase equilibria by linear programming: A tool for geodynamic modeling and its application to subduction zone decarbonation. *Earth and Planetary Science Letters* **236**, 524–541 (2005).
59. Connolly, J. A. D. The geodynamic equation of state: What and how. *Geochemistry, Geophysics, Geosystems* **10**, Q10014 (2009).
60. Xiang, H. & Connolly, J. A. D. GeoPS: An interactive visual computing tool for thermodynamic modelling of phase equilibria. *Journal of Metamorphic Geology* **40**, 243–255 (2022).
61. Holland, T. J. B. & Powell, R. An internally consistent thermodynamic data set for phases of petrological interest. *Journal of Metamorphic Geology* **16**, 309–343 (1998).
62. Holland, T. & Powell, R. A Compensated-Redlich-Kwong (CORK) equation for volumes and fugacities of CO₂ and H₂O in the range 1 bar to 50 kbar and 100–1600 °C. *Contributions to Mineralogy and Petrology* **109**, 265–273 (1991).

Acknowledgements

This project was supported by a research award from the Alexander von Humboldt foundation to BJ, by ERC Advanced Grant Agreement n°669972 to Jamtveit and ERC Consolidator Grant Agreement n°771143 to Kaus from the European Union’s Horizon 2020 Research and Innovation Programme. Parts of this research were conducted using the supercomputer MOGON2 and/or advisory services offered by Johannes Gutenberg University Mainz (hpc.uni-mainz.de), which is a member of the AHRP (Alliance for High Performance Computing in Rhineland Palatinate, www.ahrp.info) and the Gauss Alliance e.V. Andrew Putnis and Håkon Austrheim are acknowledged for numerous discussions. We would also like to acknowledge three anonymous reviewers for constructive criticism to an earlier version of the manuscript. The editor is acknowledged for the editing process.

Author contributions

All authors contributed equally in developing the main idea, writing and editing of the manuscript and analysing the results. In addition, E.M. designed the model configuration and performed the phase equilibria modelling (Fig. 3). B.K. designed the model configuration and performed all the simulations shown in Fig. 2 and in the supplementary information. B.J. contributed with his expertise on the regional geology of Norway.

Funding

Open Access funding enabled and organized by Projekt DEAL.

Competing interests

The authors declare no competing interests.

Additional information

Supplementary information The online version contains supplementary material available at <https://doi.org/10.1038/s43247-022-00478-7>.

Correspondence and requests for materials should be addressed to Evangelos Moulas.

Peer review information *Communications Earth & Environment* thanks the anonymous reviewers for their contribution to the peer review of this work. Primary Handling Editor: Joe Aslin.

Reprints and permission information is available at <http://www.nature.com/reprints>

Publisher’s note Springer Nature remains neutral with regard to jurisdictional claims in published maps and institutional affiliations.



Open Access This article is licensed under a Creative Commons Attribution 4.0 International License, which permits use, sharing, adaptation, distribution and reproduction in any medium or format, as long as you give appropriate credit to the original author(s) and the source, provide a link to the Creative Commons license, and indicate if changes were made. The images or other third party material in this article are included in the article’s Creative Commons license, unless indicated otherwise in a credit line to the material. If material is not included in the article’s Creative Commons license and your intended use is not permitted by statutory regulation or exceeds the permitted use, you will need to obtain permission directly from the copyright holder. To view a copy of this license, visit <http://creativecommons.org/licenses/by/4.0/>.

© The Author(s) 2022